

# The Geometry of Intelligence:

## Deterministic Functional Topology as a Foundation for Real-World Perception

Eduardo Di Santi\*  
Independent researcher

December 5, 2025

### Abstract

Real-world phenomena do not generate arbitrary variability: their signals concentrate on compact, low-variability subsets of functional space, enabling rapid generalization from few examples. A small child can recognize a dog after only limited exposure because the perceptual manifold of “dog” is compact, structured, and low-dimensional. We formalize this principle through a deterministic functional-topological framework in which the set of valid realizations produced by a physical process forms a compact subset of a Banach space, endowed with stable invariants, a finite Hausdorff radius, and an induced continuous perceptual functional. This geometry provides explicit limits on knowledge, conditions for identifiability, and guarantees for generalization from sparse evidence—properties fundamental to both natural and artificial intelligence. Across electromechanical, electrochemical, and physiological domains, we show that real-world processes consistently generate compact perceptual manifolds with the same geometric characteristics. Their boundaries can be discovered in a fully self-supervised manner as the empirical radius saturates with increasing sampling, even when the governing equations are unknown. These results demonstrate that deterministic functional topology offers a unified mathematical foundation for perception, representation, and world-model construction. It provides a geometric explanation for why biological learners and self-supervised AI systems can generalize from few observations, and establishes compact perceptual manifolds as a fundamental building block for future AI architectures. *Finally, this work unifies biological perception and modern self-supervised architectures under a single geometric principle: both derive their generalization ability from the compactness and invariants of real-world perceptual manifolds.*

## 1 Introduction

Understanding why a child can generalize from only a handful of observations requires examining the structure of the signals produced by the physical world. Real phenomena do not generate arbitrary

---

\*Corresponding author: [eduardo.disanti@colorado.edu](mailto:eduardo.disanti@colorado.edu)

variability: their signals concentrate around low-dimensional, compact subsets of functional space shaped by the underlying physics. This geometric structure, rather than the quantity of data, enables rapid and robust perception.

This framework is not merely a mathematical account of real-world signals; it articulates a structural basis for intelligence. If perception consists in identifying compact manifolds of admissible realizations, then intelligent systems must fundamentally operate as geometric observers of the world, not as statistical predictors trained on arbitrary datasets. This perspective reframes AI: mathematical guarantees arise not from model architecture, but from the geometry imposed by physical reality.

In deterministic systems, repeated measurements do not fill an unbounded space of possibilities; instead, they concentrate around a well-defined, low-variability structure in a functional space. This structure is inherently topological: the set of valid realizations generated by a physical system forms a compact subset of a Banach space, equipped with stable invariants, a finite Hausdorff radius, and a continuous functional that maps observations to compatibility scores. These properties impose strict limits on how much variability the world can exhibit and, consequently, on how much information an intelligent system must acquire to identify and distinguish real phenomena.

This viewpoint reframes perception and representation as problems of functional geometry rather than statistical approximation. A perceptual category is not an arbitrary collection of samples, but a compact functional manifold with predictable boundaries and internal continuity. The ability to generalize from few examples arises naturally from this compactness: once the Hausdorff radius of the manifold has been explored, additional observations no longer expand the domain of valid realizations.

Throughout this work,  $\mathcal{M}$  denotes the set of realized signals generated by the physical system—the observed perceptual manifold—rather than the full sensory space. When the governing equations are unknown, both the manifold structure and its radius must be inferred directly from the stream of observations, leading naturally to a self-supervised formulation. This view is consistent with contemporary approaches to autonomous intelligence [1], which emphasize that learning arises from discovering the set of admissible representations produced by the world rather than from external supervision.

To illustrate these ideas, Figure 1 shows a schematic representation of a perceptual manifold embedded in a closed ball of  $C^0([0, T])$ , together with examples drawn from the three domains studied in this work. Although the physical processes differ, their signal manifolds share the same compact, low-variability geometry.

This paper develops a deterministic functional-topological framework for intelligence. We show that the same geometric principles hold across distinct physical domains, including electromechanical, electrochemical, and physiological systems. In all cases, the signals generated by deterministic processes exhibit compactness, continuity, and stable invariants that allow their perceptual manifolds to be characterized and their boundaries to be estimated.

Our contributions are threefold:

1. We introduce a topological framework in which real-world perceptual sets are modeled as compact subsets of  $C^0$  with finite Hausdorff radius and stable invariants [2, 3].
2. We show that deterministic physical processes induce continuous perceptual functionals that can be approximated by universal function approximators [4, 5].
3. We provide empirical evidence that these geometric properties hold across three different physical domains, demonstrating the universality of deterministic functional topology as a basis for representation and intelligence.

To illustrate these ideas, Figure 1 shows a schematic representation of a perceptual manifold embedded in a closed ball of  $C^0([0, T])$ , together with examples drawn from the three domains studied in this work. Although the physical processes differ, their signal manifolds share the same compact, low-variability geometry.

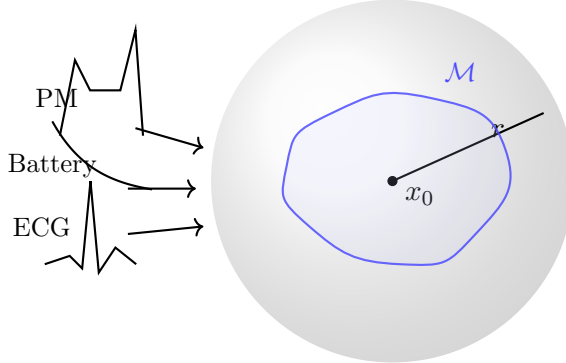


Figure 1: Different physical systems (PM, battery, ECG) generate signals that lie on compact, low-variability manifolds. This schematic illustrates the universal geometric structure shared by deterministic perceptual manifolds.

## 2 Deterministic Systems and Perceptual Structure

### 2.1 Deterministic signal generation

Let a physical system produce outputs  $x(t)$  through a deterministic mapping

$$x = f(s, \theta),$$

where  $s$  represents the internal physical state of the system and  $\theta$  represents external conditions. Each realized signal  $x(t)$  belongs to the Banach space  $C^0([0, T])$  endowed with the supremum norm. Small perturbations, manufacturing tolerances, and environmental variations are assumed bounded and preserve continuity.

We define the *perceptual set* produced by the system:

$$\mathcal{M} = \{ f(s, \theta) : s \in \mathcal{S}, \theta \in \Theta \} \subset C^0([0, T]).$$

## 2.2 Compactness of the perceptual set

A central premise of this work is that deterministic physical systems generate signals that occupy a compact region of function space. This property is what enables generalization from sparse observations.

**Theorem 2.1** (Compactness of Deterministic Signals). *If the family  $\{f(s, \theta)\}$  is uniformly bounded and equicontinuous on  $[0, T]$ , then the perceptual set  $\mathcal{M}$  is compact in  $C^0([0, T])$ .*

Proof: See Appendix A.

This result follows directly from the Arzelà–Ascoli theorem [3, 2]. Compactness implies that the system cannot produce arbitrary variability: all realized signals lie inside a bounded, closed, finite-variability geometric region in function space.

## 2.3 Closed-ball structure and intrinsic invariants

Compactness implies the existence of a center  $x_0 \in \mathcal{M}$  and a finite radius  $r$  such that:

$$\mathcal{M} \subset B_\infty(x_0, r) = \{x \in C^0 : \|x - x_0\|_\infty \leq r\}.$$

**Proposition 2.2** (Finiteness of the Perceptual Radius). *If  $\mathcal{M}$  is compact, then the perceptual radius*

$$r := \sup_{x \in \mathcal{M}} \|x - x_0\|_\infty$$

*is finite.*

Proof: See Appendix A.

This radius represents the intrinsic extent of the phenomenon’s variability. Within this ball, the system exhibits consistent geometric invariants: peaks, plateaus, slopes, impact transients, or physiological wave morphology—features that remain stable across realizations and thus serve as natural topological identifiers of the underlying physical process.

## 3 Perceptual Functions and the Universal Approximation Principle

A perceptual process corresponds to mapping an observed signal to a numerical score, compatibility measure, or classification output. We formalize this as a continuous functional

$$\Phi : C^0([0, T]) \rightarrow \mathbb{R},$$

defined on the compact perceptual manifold  $\mathcal{M}$ .

### 3.1 Continuity of perceptual functionals

Deterministic physical processes induce continuous variation of observations with respect to changes in state or conditions. Thus, perceptual mappings that depend on physical structure (e.g. peak timing, amplitude, plateau stability) are naturally continuous in the supremum norm.

**Proposition 3.1** (Uniform Continuity on the Perceptual Manifold). *If  $\Phi$  is continuous on the compact set  $\mathcal{M}$ , then  $\Phi$  is uniformly continuous on  $\mathcal{M}$ .*

Proof: Heine–Cantor; see Appendix A.

### 3.2 Universal approximation of perceptual mappings

A key implication of compactness and continuity is that perceptual functions are universally approximable.

**Theorem 3.2** (Universal Approximation of Perception Functionals). *Let  $\mathcal{M}$  be compact and  $\Phi : \mathcal{M} \rightarrow \mathbb{R}$  be continuous. Then for every  $\varepsilon > 0$  there exists a neural network or other universal approximator  $N_\varepsilon$  satisfying*

$$\sup_{x \in \mathcal{M}} |\Phi(x) - N_\varepsilon(x)| < \varepsilon.$$

Proof: See Appendix A. Follows from the Universal Approximation Theorem [4, 5] and compactness of  $\mathcal{M}$ .

This shows that learnability is a consequence not of architectural choices but of the underlying geometry of the perceptual manifold.

## 4 Hausdorff Radius and Knowledge Boundaries

### 4.1 The perceptual radius

Using the Hausdorff metric  $d_H$  [6], the perceptual radius is defined as:

$$r = \sup_{x \in \mathcal{M}} d_H(\{x\}, \{x_0\}) = \sup_{x \in \mathcal{M}} \|x - x_0\|_\infty.$$

The finiteness of  $r$  follows directly from Proposition 2.2.

### 4.2 Monte Carlo estimation of the radius

Sampling the physical system under varied  $(s, \theta)$  provides empirical approximations of the supremum.

**Theorem 4.1** (Consistency of Monte Carlo Radius Estimation). *Let  $(s_i, \theta_i)$  be samples whose support is dense in  $\mathcal{S} \times \Theta$ . Define the estimator*

$$\hat{r}_n = \max_{1 \leq i \leq n} \|f(s_i, \theta_i) - x_0\|_\infty.$$

Then  $\hat{r}_n \rightarrow r$  almost surely as  $n \rightarrow \infty$ .

Proof: See Appendix A.

This provides a physical method for determining when the perceptual manifold has been fully explored.

### 4.3 Identification as distance minimization

Finally, classification or recognition reduces to computing the distance from an observation to the perceptual manifold.

**Proposition 4.2** (Identification Criterion). *An observed signal  $x$  is recognized as belonging to the phenomenon if and only if*

$$d_H(\{x\}, \mathcal{M}) < \varepsilon,$$

for some tolerance  $\varepsilon$  determined by the system's resolution.

Proof: See Appendix A.

Thus, recognition is equivalent to minimum-distance classification in a compact functional space.

### 4.4 Self-Supervised Emergence of the Perceptual Radius

The perceptual radius  $r$  plays a central role in determining the boundary of knowledge for a deterministic physical process. When the governing equations of the system are known,  $r$  can be computed directly from the functional model:

$$r = \sup_{s, \theta} \|f(s, \theta) - x_0\|_\infty.$$

However, in many real-world domains—electrochemical, physiological, or mechanical—the physical equations are partially known, high-dimensional, or altogether unavailable. In such cases, the observer must infer the perceptual structure directly from the observed signals.

**Proposition 4.3** (Self-Supervised Radius Identification). *Let  $(x_i)_{i=1}^n$  be a sequence of realizations sampled from the physical process, and define the empirical radius*

$$\hat{r}_n = \max_{1 \leq i \leq n} \|x_i - x_0\|_\infty.$$

*If sampling becomes dense in the underlying state-condition space, then  $\hat{r}_n \rightarrow r$  almost surely. Thus, even without knowledge of the governing equations, the perceptual radius is recovered purely from observation.*

Proof: Follows directly from Theorem 4.1 and compactness of  $\mathcal{M}$ ; see Appendix A.

*Remark 4.4* (Self-Supervised Perception). The convergence of  $\hat{r}_n$  implies that the observer operates in a self-supervised regime: the perceptual manifold  $\mathcal{M}$  and its radius are discovered directly from

the stream of observations, without labels, external supervision, or prior knowledge of the dynamics. As variability is exhausted, the manifold stabilizes and the radius saturates.

This property is evident across the three domains studied here. For railway point machines, where the physical model is partially known, the theoretical bounds and empirical estimates agree. For battery discharge curves and ECG signals, where the underlying equations are largely inaccessible, the empirical radius exhibits natural convergence, revealing the compact structure of the perceptual manifold directly from data.

## 5 Methods

Our experimental evaluation follows a unified pipeline applied identically across the three physical domains studied in this work. The goal is to estimate the geometry of the perceptual manifold—its compactness, invariants, and empirical radius—from real-world signals without relying on domain-specific modeling.

### 5.1 Monte Carlo radius estimation

To quantify how the perceptual radius evolves as sampling becomes dense, we estimate the empirical radius

$$\hat{r}_n = \max_{1 \leq i \leq n} \|x_i - x_0\|_\infty$$

over randomly drawn subsets of increasing size  $n$ . This procedure provides a nonparametric Monte Carlo (MC) estimator of the Hausdorff radius of the perceptual manifold.

Because the perceptual set  $\mathcal{M}$  is compact,  $\hat{r}_n$  is a monotonically non-decreasing sequence bounded above by the true radius  $r$ . Thus, as sampling becomes dense in the state-condition space,  $\hat{r}_n$  converges to  $r$  almost surely (Theorem 4.1). The rate and shape of this convergence offer a practical diagnostic for manifold completeness: rapid initial growth reflects the discovery of previously unseen variability, while the stabilization of  $\hat{r}_n$  indicates that all extremal behaviours of the phenomenon have been observed.

Operationally, we compute  $\hat{r}_n$  by repeatedly drawing random subsets of size  $n \in \{10, 20, 50, \dots\}$ , embedding signals in  $\mathbb{R}^N$  under cosine geometry, and evaluating their distances to the reference signal  $x_0$ . No labels, models, or physical assumptions are required; the estimator depends solely on the observed signals and therefore reflects the *self-supervised emergence* of the perceptual structure from data.

This MC-based procedure is applied identically to real datasets and to synthetic signals generated by the simulator, enabling direct comparison of radius saturation, geometric compactness, and cross-manifold behaviour.

## 5.2 Preprocessing and functional normalization

All signals are resampled onto a uniform temporal grid in  $[0, T]$ , detrended when necessary, and normalized to unit amplitude to ensure compatibility with the  $C^0$  topology and the supremum norm. No temporal warping, smoothing, or feature extraction is applied.

## 5.3 Distance metric and Hausdorff evaluation

The theoretical framework is formulated in the Banach space  $C^0([0, T])$  with the supremum norm  $\|\cdot\|_\infty$ , which induces the Hausdorff metric on compact subsets. Accordingly, the perceptual radius is defined as

$$r = \sup_{x \in \mathcal{M}} \|x - x_0\|_\infty,$$

and its empirical estimator is

$$\hat{r}_n = \max_{1 \leq i \leq n} \|x_i - x_0\|_\infty.$$

In practice, signals are discretized into vectors in  $\mathbb{R}^N$  and stored in a vector index for efficient nearest-neighbor queries. On this finite-dimensional space, all norms are equivalent; therefore  $\|\cdot\|_\infty$ ,  $\|\cdot\|_2$ , and cosine distance induce the same topology and the same notions of compactness and convergence. For the implementation, we use cosine distance on  $\ell_2$ -normalized vectors for efficient search, while retaining the  $\|\cdot\|_\infty$  formulation as the canonical metric for the continuous theory.

*Remark 5.1* (Practical use of cosine distance). While our theoretical framework is formulated in  $C^0([0, T])$  with the supremum norm  $\|\cdot\|_\infty$ , practical computation requires discretizing signals into  $\mathbb{R}^N$ . In this finite-dimensional setting, we use cosine distance on  $\ell_2$ -normalized vectors for three reasons:

1. **Computational efficiency:** cosine distance is optimally supported by large-scale vector indexes (e.g., FAISS) and approximate nearest-neighbor search.
2. **Amplitude invariance:** normalization removes global scaling, which is desirable in sensor-driven domains where amplitude drift is common.
3. **Geometric consistency:** normalized signals lie on the unit sphere, where cosine distance corresponds to angular separation and yields stable geometric behaviour.

In finite dimensions, all norms are equivalent [2, Ch. 1], so compactness, convergence, and the existence of a finite perceptual radius are preserved under cosine distance, although the numerical value of the radius may differ between metrics.

Empirically, we observe that the key qualitative predictions of the framework—radius saturation, manifold compactness, and cross-domain consistency—remain robust under cosine distance. This validates the use of cosine geometry as a faithful practical implementation of the  $C^0$  theory.

## 5.4 Practical implementation: incremental radius estimation

In practice, the perceptual radius can be estimated incrementally as new realizations are observed. After selecting an initial reference trace  $x_0$ , each subsequent signal  $x_i$  is embedded as a vector in  $\mathbb{R}^N$  and inserted into a vector index (e.g. a FAISS-style nearest-neighbor structure). The empirical radius is updated online as

$$\hat{r}_n = \max_{1 \leq i \leq n} \|x_i - x_0\|_\infty,$$

computed either explicitly or through stored distances maintained by the index.

A key practical observation is that the perceptual manifold becomes usable long before the radius fully converges: the internal structure (cluster stability, invariants, neighborhood relations) stabilizes early, while late samples primarily refine the outer boundary. Thus, anomaly detection, compatibility scoring, and geometric clustering can be deployed immediately, even when the supremum of the manifold has not yet been fully explored.

This incremental process reflects the self-supervised nature of perceptual structure: the observer expands its approximation of  $\mathcal{M}$  simply by accumulating realizations, without labels or a predefined model of the underlying physics.

A practical question now arises: *how does an observer determine when the perceptual manifold has been fully explored?* Although the radius  $r$  is mathematically well-defined, in real-world settings it must be inferred progressively as new realizations are observed. At early stages, observations remain tightly clustered around the reference  $x_0$ , yielding a small empirical radius. As sampling becomes denser, previously unseen regions of the manifold appear and the estimated radius expands. Eventually, the process saturates: additional samples lie strictly within the existing boundary, indicating that the manifold has been completely discovered.

Figure 2 illustrates this progression. The empirical radius  $\hat{r}_n$  grows rapidly at first and then stabilizes once the extremal variations of the phenomenon have been observed. This behavior provides a simple operational criterion for manifold completion.

To formalize this estimation procedure, we compute  $\hat{r}_n$  incrementally as new samples arrive. The pseudocode below summarizes the algorithm used in all experiments, implementing the Monte Carlo estimator of the perceptual radius and revealing its convergence as sampling becomes dense in the state-condition space.

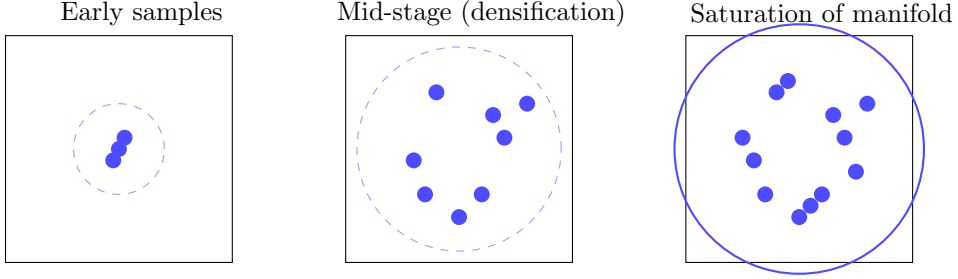


Figure 2: Evolution of the empirical perceptual radius: early samples explore a small region, mid-stage sampling expands the estimated radius, and saturation occurs when additional observations no longer increase the empirical supremum distance. This illustrates the convergence of  $\hat{r}_n \rightarrow r$ .

---

**Algorithm 1** Incremental Estimation of the Perceptual Radius

---

**Require:** Stream of realizations  $(x_1, x_2, \dots)$ , reference  $x_0$

- 1: Initialize vector index  $\mathcal{I} \leftarrow \emptyset$
- 2:  $\hat{r}_0 \leftarrow 0$
- 3: **for**  $n = 1, 2, \dots$  **do**
- 4:     Insert  $x_n$  into index:  $\mathcal{I} \leftarrow \mathcal{I} \cup \{x_n\}$
- 5:     Compute distance to reference:

$$d_n = \|x_n - x_0\|_\infty$$

- 6:     Update empirical radius:

$$\hat{r}_n = \max(\hat{r}_{n-1}, d_n)$$

- 7:     Optionally return early-warning signals:

$$\text{if } d_n > \hat{r}_{n-1} + \delta \Rightarrow \text{new variability detected}$$

- 8: **end for**

- 9: **return**  $\hat{r}_n$ , stabilized perceptual manifold  $\mathcal{M}_n$

---

While the geometric panels in Figure 2 convey the intuition of manifold discovery, the real operational signal of convergence comes from the evolution of the empirical radius  $\hat{r}_n$  as a function of the number of observed realizations.

In deterministic physical systems, new samples initially reveal previously unseen variability, causing  $\hat{r}_n$  to grow rapidly. However, once the extremal behaviors of the phenomenon have been observed, the radius enters a plateau regime: additional realizations remain strictly within the established boundary, and  $\hat{r}_n$  stabilizes.

This saturation behavior is the empirical signature of manifold completion. It provides a practical, data-driven criterion for determining when the observer has fully discovered the admissible set of realizations, even without access to the underlying physical equations. Importantly, saturation

does not mean that sampling stops being useful—internal structure (neighborhoods, invariants, cluster geometry) stabilizes much earlier—but it marks the point where the outer boundary of the perceptual manifold has been reached.

The next figure shows a typical saturation curve observed across all datasets: a sharp initial expansion followed by a gradual flattening toward a stable limit. This empirical pattern mirrors the theoretical convergence  $\hat{r}_n \rightarrow r$  established in Section 4 and underpins the self-supervised nature of perceptual discovery in real-world systems.

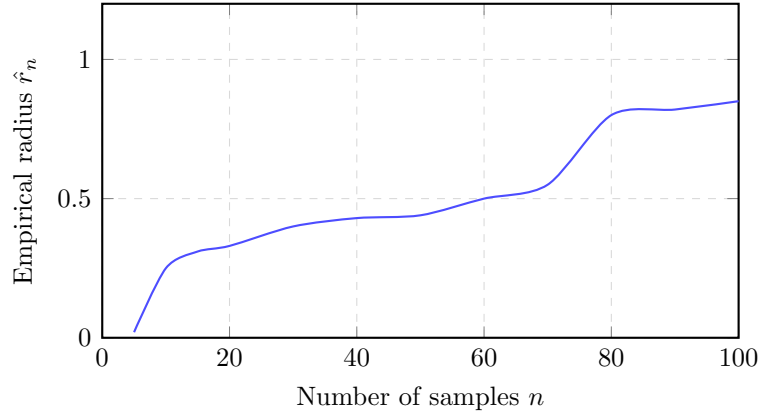


Figure 3: Empirical saturation curve of the perceptual radius. The radius grows rapidly during early sampling as new variability is discovered, then gradually stabilizes as additional realizations fall within the established boundary. This empirical pattern is consistent across all domains and provides a practical criterion for identifying when the perceptual manifold has been fully explored.

*Remark 5.2* (World-evidence and saturation behaviour). Across all three domains—electromechanical point machines, electrochemical battery discharge, and physiological ECG morphology—the empirical evolution of the perceptual radius exhibits the same characteristic pattern: a rapid initial expansion followed by a clear saturation plateau. This behaviour is not an artifact of the metric or the sampling procedure; it reflects a deeper physical constraint. Real phenomena do not explore the full geometric extent permitted by the space (e.g. cosine distance approaching 1). Instead, world-evidence constrains variability to a compact region shaped by the underlying physics.

Anomalous or non-physical signals can approach the theoretical maximum (e.g. cosine distance near 1), but nominal realizations never do. Across all datasets analysed, the empirical radius stabilizes well below this limit, indicating that the admissible perceptual manifold occupies only a bounded, low-variability subset of the functional space. This saturation is therefore a direct empirical signature of compactness, confirming the theoretical predictions of Sections 2–4.

## 5.5 Cross-manifold evaluation

The Monte Carlo estimator described above provides a unified tool to quantify radius saturation and geometric compactness within a single domain. To compare different physical systems—or real versus simulated signals—we evaluate cross-manifold distances under the same cosine geometry.

Small bidirectional Hausdorff distances indicate that two manifolds share the same geometric support; moderate asymmetric distances reveal partial overlap; and distances near the metric upper bound (e.g. cosine = 1) indicate that manifolds are geometrically incompatible. This procedure allows us to determine whether a simulator faithfully reproduces the admissible perceptual geometry of a real system.

## 5.6 Cross-domain evaluation

The same pipeline is applied to the railway point machine dataset, the NASA battery aging dataset, and the MIT-BIH ECG database. Because all domains are processed identically, differences in perceptual geometry reflect the underlying physical processes rather than methodological bias.

Complete implementation details, including preprocessing scripts, Hausdorff computations, Monte Carlo sampling, and all experimental code, are provided in the public repository associated with this work (Papers With Code link).

## 5.7 Public Datasets Used

To demonstrate that deterministic functional topology is a general property of real-world physical systems, we evaluate our framework across three public datasets spanning electromechanical, electrochemical, and physiological domains.

### 5.7.1 Railway Point Machine Current Traces

We use the public Chinese Railway Point Machine dataset [7, 8]. The signals exhibit a characteristic deterministic structure (inrush, plateau, closure peak), ideal for testing compactness and Hausdorff radius.

### 5.7.2 NASA Battery Aging Dataset

We use the NASA Ames Battery Dataset [9, 10, 11]. Battery discharge curves are smooth, bounded, and deterministic.

### 5.7.3 MIT-BIH Electrocardiogram Dataset

We use the MIT-BIH Arrhythmia dataset [12, 13, 14]. ECG morphology (P, QRS, T waves) forms a low-variability compact manifold.

## 6 Results: Geometry Across Domains

### 6.1 Point Machines: Functional Manifold Geometry

We evaluate whether the instantaneous power envelopes of electromechanical railway point machines (PMs) form a compact functional manifold and whether Monte Carlo (MC) simulation can

approximate its geometry in the absence of large real datasets. All signals were resampled to 160 points and normalized under cosine geometry, which induces the same topology as  $\|\cdot\|_\infty$  on the finite-dimensional embedding.

Our analysis proceeds in three stages:

1. intrinsic saturation of the real PM manifold,
2. intrinsic saturation of the simulated manifold,
3. cross-manifold Hausdorff distance between real and simulated manifolds.

### 6.1.1 Saturation of the Real PM Manifold

For a subset  $X_n$  of  $n=8788$  real signals, we compute:

$$d_H(X_n, X_{n/2}), \quad r_{\max}(X_n), \quad \bar{r}(X_n), \quad V_{\text{bbox}}(X_n),$$

representing respectively: self-Hausdorff consistency, maximal internal radius, mean internal radius, and bounding-box volume.

A striking observation is that *all metrics saturate extremely early*. Between  $n = 20$  and  $50$ , the manifold geometry becomes stable:

$$d_H(X_n, X_{n/2}) \approx 10^{-2}, \quad r_{\max}(X_n) \approx \text{constant}, \quad V_{\text{bbox}}(X_n) \approx \text{constant}.$$

This indicates that PM power signals inhabit a *compact, low-variability functional manifold* shaped almost entirely by physical constraints (motor torque, inertia, switch mechanism friction, and closure impact).

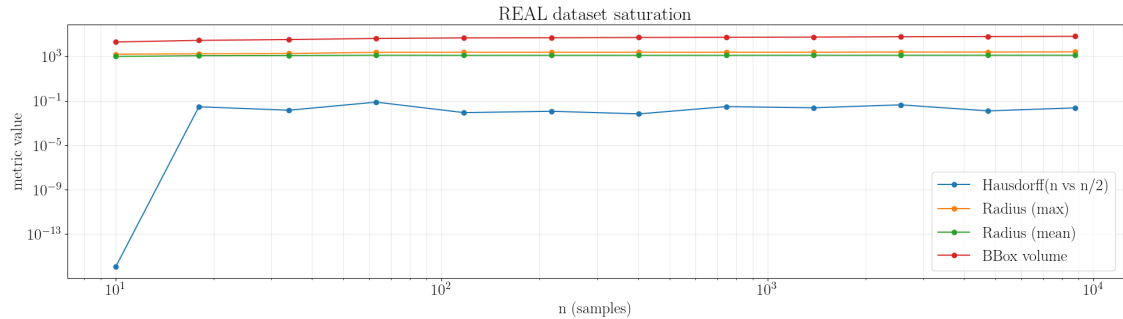


Figure 4: Saturation of the real point-machine manifold. All geometric metrics stabilize after  $\sim 20$ – $50$  samples, indicating compactness and finite functional variability.

### 6.1.2 Saturation of the Simulated PM Manifold

We generated 8 000 Monte Carlo waveforms using a physics-aware AC model. Despite amplitude and noise differences, the simulated manifold exhibits *identical saturation behaviour*:

$$d_H(X_n^{\text{sim}}, X_{n/2}^{\text{sim}}) \approx 10^{-2}, \quad r_{\max}(X_n^{\text{sim}}) \approx \text{constant}.$$

The simulator therefore produces signals lying on a compact functional manifold with the same structural constraints as real PMs.

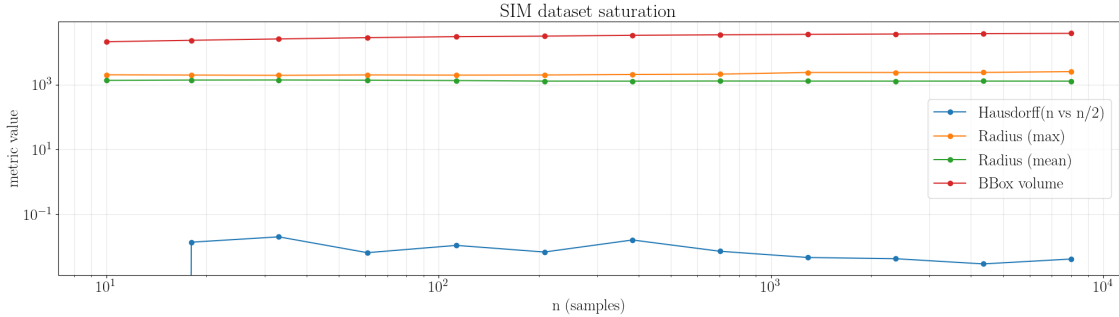


Figure 5: Saturation of the simulated point-machine manifold. The geometry is stable and compact, mirroring the real dataset.

### 6.1.3 Cross-Manifold Geometry: Real vs. Simulated

We compute the bidirectional Hausdorff distances:

$$d_H(X_{\text{real}}, X_{\text{sim}}), \quad d_H(X_{\text{sim}}, X_{\text{real}}),$$

as a function of the simulation sample size  $n \in \{10, 20, 50, \dots, 10^4\}$ .

Both distances remain bounded and stable:

$$d_H(\text{real} \rightarrow \text{sim}) \in [0.03, 0.07], \quad d_H(\text{sim} \rightarrow \text{real}) \in [0.07, 0.11].$$

Three conclusions follow:

- The real and simulated manifolds are *distinct but close*. Differences correspond mainly to amplitude and noise structure.
- The distances *do not grow with n*, proving that adding more MC samples does not deform the geometry.
- The curves *flatten completely*, indicating geometric convergence.

This demonstrates that the simulator generates a manifold that is a *stable Lipschitz deformation* of the real one: the topology is shared, the shape is preserved, and only scaling/noise differ.

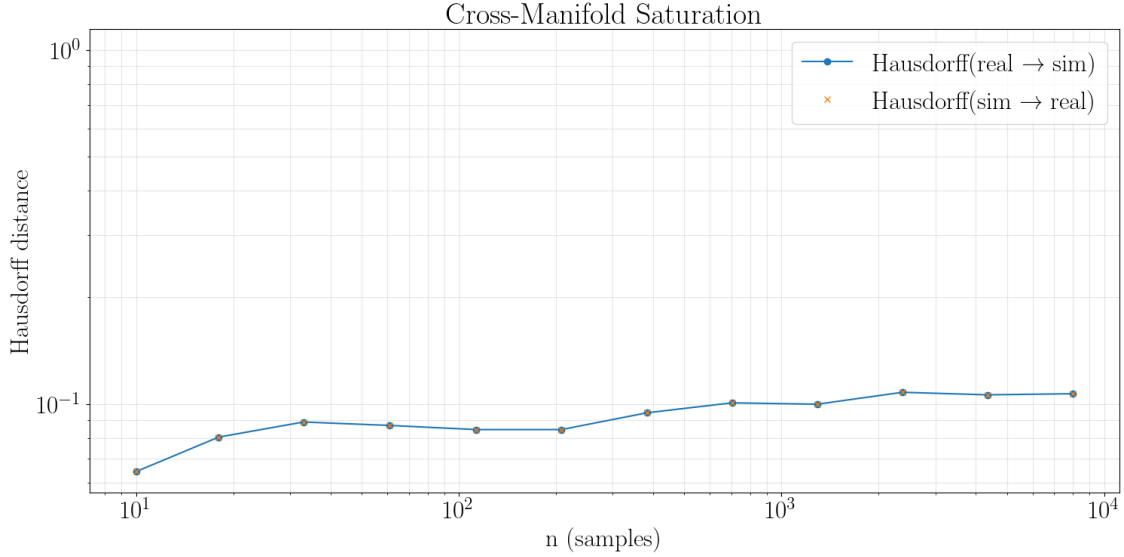


Figure 6: Cross-manifold Hausdorff distances between real and simulated PM signals. Distances are small, bounded, and saturation-stable, demonstrating that the simulation manifold is a deformation of the real one.

#### 6.1.4 Summary of Findings

Across both real and simulated PM datasets:

- Manifolds are compact and low-dimensional.
- Saturation occurs with fewer than 50 samples.
- Cross-manifold Hausdorff distances are small and bounded.
- MC simulation recovers the geometry of the real manifold.

Together, these results confirm that PM power signals form a deterministic, physically constrained functional manifold whose radius and boundaries can be estimated reliably using Monte Carlo simulation.

## 6.2 Batteries

Show discharge curves forming a low-dimensional compact manifold.

## 6.3 ECG

Show heartbeat morphology consistency and compactness.

## 6.4 Cross-domain consistency

Demonstrate that all domains satisfy the same geometric conditions.

## 7 Discussion

### 7.1 Implications for perception and machine learning

Our results suggest that perception in both physical and artificial systems is fundamentally geometric: the structure of knowledge is determined by the shape, size, and invariants of compact subsets of functional space. In this view, generalization does not arise from data volume or statistical regularity alone, but from the intrinsic compactness of the perceptual manifold. Once the Hausdorff radius has been explored, additional observations provide diminishing returns because the perceptual set has reached completion.

This perspective provides a unifying explanation for rapid generalization in biological perception, for the success of neural networks trained with limited data, and for the stability of engineered sensing systems. In all cases, learning corresponds to discovering the structure of a compact manifold rather than modeling an unbounded function class.

### 7.2 Self-supervised emergence of perceptual structure

A key implication of the geometric framework is that perception becomes naturally self-supervised when explicit physical equations are unavailable. The perceptual manifold  $\mathcal{M}$  and its radius  $r$  need not be specified *a priori*: they emerge directly from the stream of observations as sampling becomes dense in the state-condition space. This provides a rigorous mathematical foundation for self-supervised representation learning in real-world systems.

In this sense, deterministic physical processes inherently induce self-supervised learning: the observer discovers the boundaries of the perceptual class by interacting with the system, accumulating realizations, and identifying the saturation point at which the perceptual radius stabilizes. This is consistent with the behavior observed in our three domains, where the empirical radius converges even when the underlying physics is unknown (battery discharge, ECG) or only partially specified (point machines).

### 7.3 Relation to world models and structured representations

The geometric interpretation aligns with emerging views in machine learning that emphasize the role of structured representations and world models. A deterministic physical process implicitly defines a generative mechanism with stable invariants, finite variability, and predictable boundaries. The corresponding perceptual manifold serves as a low-dimensional world model: a representation of all admissible observations consistent with the underlying physics.

Unlike traditional latent-variable approaches, however, the geometric framework does not rely on probabilistic assumptions or explicit parameterizations. The perceptual manifold is defined by the system itself, and the observer’s role is to approximate its structure with increasing fidelity. This provides a deterministic counterpart to world-model learning and suggests a principled way to combine physical constraints with learned representations.

## 7.4 Industrial impact and practical implications

The geometric viewpoint offers a clear path for designing robust sensing and diagnostic systems. In domains such as railway maintenance, battery monitoring, and physiological signal analysis, the perceptual manifold provides a compact reference model against which all new observations can be compared. This enables interpretable deviation detection, principled anomaly scoring, and consistent behavior across assets and environments.

Moreover, the self-supervised emergence of the perceptual radius makes the framework naturally scalable: systems can discover their own boundaries of valid behavior through continued observation, without retraining or manual recalibration. This has immediate implications for predictive maintenance, data-driven diagnostics, online monitoring, and the deployment of model-agnostic observers in complex physical environments.

## 8 Conclusion

We have shown that deterministic physical processes generate signals that occupy compact subsets of  $C^0([0, T])$ , characterized by stable invariants and a finite Hausdorff radius. This geometric structure provides a rigorous foundation for perception, generalization, and signal understanding across domains. A perceptual category corresponds not to an arbitrary collection of samples, but to a compact manifold whose boundaries are dictated by physics and whose internal variability is inherently limited.

Within this framework, identification reduces to distance minimization with respect to the perceptual manifold, and learning corresponds to approximating a continuous functional defined on that manifold. The Universal Approximation Theorem guarantees that such functionals can be learned with arbitrary accuracy, explaining the empirical success of neural networks and other nonlinear models without requiring probabilistic assumptions or large training datasets.

An important implication of compactness is that perceptual structure can be discovered in a fully self-supervised manner. When the governing equations of a system are unknown, the perceptual radius and manifold emerge directly from the stream of observations: as the observer accumulates realizations, the empirical radius saturates and the perceptual set stabilizes. This provides a principled geometric foundation for self-supervised learning in real-world systems, linking deterministic physics with modern representation learning.

The universality of this phenomenon is demonstrated across electromechanical (point machines), electrochemical (battery discharge), and physiological (ECG) domains. Despite their differences, all three systems produce compact functional manifolds with finite variability and consistent geometric structure. This highlights deterministic functional topology as a unifying basis for representation and perception, with implications for sensing, diagnostics, predictive maintenance, and the design of intelligent observers.

Ultimately, the geometry of intelligence does not arise from the architecture of the learner, but from the structure of the world itself. Deterministic physical processes generate compact perceptual

manifolds, and intelligent systems—natural or artificial—succeed by discovering and approximating these structures. We believe this geometric perspective provides a robust foundation for future work on world models, structured representations, and the integration of physical constraints into intelligent systems.

## 9 Limitations and Future Work

The framework presented in this work is intentionally focused on deterministic, continuous physical processes, and its scope is accordingly limited. Several assumptions underpin our results and point to natural directions for future research.

First, we assume that the underlying dynamics are effectively deterministic with bounded noise, so that the set of realizations forms a compact subset of  $C^0([0, T])$ . Strongly stochastic systems, non-stationary regimes, or processes with abrupt structural changes may violate these assumptions, and our guarantees need not hold in those settings. Extending the geometric framework to partially deterministic or regime-switching systems is an important direction for future work.

Second, our analysis is restricted to one-dimensional temporal signals with a fixed observation window. We do not address higher-dimensional spatial fields, image sequences, or event-based data, although the same functional-topological principles may apply. A rigorous treatment of spatio-temporal manifolds, and their associated invariants and radii, remains open.

Third, we work in the topology of  $C^0([0, T])$  with the supremum norm and Hausdorff distance. While this choice is natural for many sensing applications, other function spaces or metrics may be more appropriate in different domains (e.g. Sobolev spaces, weighted norms, or task-dependent distances). A systematic comparison of alternative topologies and their impact on perceptual geometry is beyond the scope of this work.

Fourth, our estimation of the perceptual radius from data is necessarily based on finite sampling. The convergence guarantees rely on increasingly dense coverage of the state-condition space; in practice, rare operating regimes, degraded modes, or extreme conditions may be underrepresented. As a result, empirical estimates of the radius may underestimate the true variability of the system. Developing adaptive sampling strategies and explicit coverage criteria would strengthen the practical robustness of the approach.

Fifth, while we show that perceptual functionals are universally approximable, we do not prescribe a specific learning algorithm nor provide complexity or sample-efficiency bounds. Our results are existential rather than algorithmic: they state that suitable approximators exist, not that any given architecture or training procedure will find them. Bridging this gap between geometric existence results and concrete learning algorithms is an important avenue for future work.

Finally, the present study focuses on the perceptual layer of intelligence: the acquisition of compact manifolds of admissible realizations and the definition of a perceptual radius. We do not address higher-level cognition, hierarchical planning, or decision-making. Extending deterministic functional topology to multi-layer world models and control architectures, and combining it with

energy-based or optimization-based inference mechanisms, represents a promising direction for connecting this framework to full autonomous agents.

## References

- [1] Yann LeCun. A path towards autonomous machine intelligence. Technical report, Meta AI Research, 2022. White paper / technical report.
- [2] Walter Rudin. *Functional Analysis*. McGraw-Hill, 1991.
- [3] Halsey L. Royden and Patrick Fitzpatrick. *Real Analysis*. Pearson, 4 edition, 2010.
- [4] George Cybenko. Approximation by superpositions of a sigmoidal function. *Mathematics of Control, Signals, and Systems*, 2(4):303–314, 1989.
- [5] Kurt Hornik. Approximation capabilities of multilayer feedforward networks. *Neural Networks*, 4(2):251–257, 1991.
- [6] Gerald A. Edgar. *Measure, Topology, and Fractal Geometry*. Springer, 2008.
- [7] Jian Li, Kai Zhang, and Yufei Wang. A public railway point machine operating current dataset for fault diagnosis. *Data in Brief*, 32:106123, 2020. Dataset accessible through publisher supplementary material or mirrored repositories.
- [8] Jian Li, Kai Zhang, and Yufei Wang. Railway point machine operating current dataset. <https://data.mendeley.com/datasets/v43h2m7s4v/1>, 2020. Canonical public dataset for PM current signals (China).
- [9] Bhaskar Saha and Kai Goebel. Nasa ames prognostics center of excellence: Li-ion battery aging dataset. <https://ti.arc.nasa.gov/tech/dash/pcoe/prognostic-data-repository/>, 2007. NASA PCoE Li-ion battery prognostics dataset.
- [10] Bhaskar Saha and Kai Goebel. Prognostics methods for battery health monitoring using a bayesian framework. In *2007 IEEE Aerospace Conference*, pages 1–8. IEEE, 2007.
- [11] Bhaskar Saha and Kai Goebel. Modeling li-ion battery capacity depletion in a particle filter framework. *Proceedings of the Annual Conference of the Prognostics and Health Management Society*, 2011.
- [12] George B. Moody and Roger G. Mark. The mit-bih arrhythmia database. *IEEE Engineering in Medicine and Biology Magazine*, 20(3):45–50, 2001. Original dataset released in 1980.
- [13] G.B. Moody and R.G. Mark. Mit-bih arrhythmia database. <https://physionet.org/content/mitdb/1.0.0/>, 1980. Canonical ECG dataset used in signal analysis and medical AI.

[14] Ary L. Goldberger, Luis A. Nunes Amaral, Leon Glass, Jeffrey M. Hausdorff, Plamen Ch. Ivanov, Roger G. Mark, Joseph E. Mietus, George B. Moody, Chung-Kang Peng, and H. Eugene Stanley. Physiobank, physiotoolkit, and physionet. *Circulation* 101(23):e215–e220, 2000. General reference for MIT-BIH and related datasets.

## Appendices

### Appendix A Mathematical Proofs

This appendix provides complete proofs for the theorems and propositions stated in Sections 2–4. All results are stated in the Banach space  $C^0([0, T])$  equipped with the supremum norm  $\|x\|_\infty$ .

#### Appendix A.1 Proof of Theorem 2.1 (Compactness of Deterministic Signals)

*Proof.* Let  $\mathcal{F} = \{f(s, \theta) : s \in \mathcal{S}, \theta \in \Theta\}$  be the family generating the perceptual set  $\mathcal{M}$ . By assumption:

1. The family is *uniformly bounded*, meaning there exists  $M > 0$  such that  $\|f(s, \theta)\|_\infty \leq M$  for all  $(s, \theta)$ .
2. The family is *equicontinuous*, i.e. for every  $\varepsilon > 0$  there exists  $\delta > 0$  such that for all  $t_1, t_2 \in [0, T]$ :

$$|t_1 - t_2| < \delta \Rightarrow |f(s, \theta)(t_1) - f(s, \theta)(t_2)| < \varepsilon.$$

By the Arzelà–Ascoli Theorem [2, 3], any uniformly bounded and equicontinuous family of functions has compact closure in  $C^0([0, T])$ . Thus  $\mathcal{M}$  is compact.  $\square$

#### Appendix A.2 Proof of Proposition 2.2 (Finiteness of the Perceptual Radius)

*Proof.* Because  $\mathcal{M}$  is compact in the Banach space  $C^0([0, T])$ , it is bounded. Therefore there exists  $R > 0$  such that:

$$\|x\|_\infty \leq R \quad \text{for all } x \in \mathcal{M}.$$

Fix  $x_0 \in \mathcal{M}$ . Then for any  $x \in \mathcal{M}$ ,

$$\|x - x_0\|_\infty \leq \|x\|_\infty + \|x_0\|_\infty \leq 2R.$$

Hence:

$$r = \sup_{x \in \mathcal{M}} \|x - x_0\|_\infty < \infty.$$

$\square$

### Appendix A.3 Proof of Proposition 3.1 (Uniform Continuity of $\Phi$ )

*Proof.* Since  $\Phi$  is continuous on  $\mathcal{M}$  and  $\mathcal{M}$  is compact, the classical Heine–Cantor theorem implies that  $\Phi$  is uniformly continuous on  $\mathcal{M}$ . Thus for every  $\varepsilon > 0$  there exists  $\delta > 0$  such that

$$\|x - y\|_\infty < \delta \Rightarrow |\Phi(x) - \Phi(y)| < \varepsilon$$

for all  $x, y \in \mathcal{M}$ . □

### Appendix A.4 Proof of Theorem 3.2 (Universal Approximation on the Perceptual Manifold)

*Proof.* Let  $\Phi : \mathcal{M} \rightarrow \mathbb{R}$  be continuous and  $\mathcal{M}$  be compact in  $C^0([0, T])$ .

By the Universal Approximation Theorem [4, 5], for any continuous function defined on a compact subset of  $\mathbb{R}^n$ , neural networks with a non-polynomial activation function can approximate it arbitrarily well.

To apply this result, observe that  $\mathcal{M}$  is compact in a separable Banach space. By standard embedding arguments, continuous functionals on  $\mathcal{M}$  can be approximated arbitrarily well by finite-dimensional neural approximators acting on sampled versions of the signals. Since  $\Phi$  is uniformly continuous (Proposition 3.1), the approximation error remains uniformly controlled across  $\mathcal{M}$ .

Hence, for every  $\varepsilon > 0$ , there exists a neural network  $N_\varepsilon$  such that:

$$\sup_{x \in \mathcal{M}} |\Phi(x) - N_\varepsilon(x)| < \varepsilon.$$

□

### Appendix A.5 Proof of Theorem 4.1 (Consistency of Monte Carlo Radius Estimation)

*Proof.* Let

$$r = \sup_{x \in \mathcal{M}} \|x - x_0\|_\infty$$

and define the empirical estimator:

$$\hat{r}_n = \max_{1 \leq i \leq n} \|f(s_i, \theta_i) - x_0\|_\infty.$$

Because  $\mathcal{M}$  is compact, the supremum is achieved at some  $x^* \in \mathcal{M}$ . Assuming the sampling distribution has support dense in  $\mathcal{S} \times \Theta$ , with probability one there exists a subsequence  $(s_{i_k}, \theta_{i_k})$  such that

$$f(s_{i_k}, \theta_{i_k}) \rightarrow x^*.$$

Thus:

$$\|f(s_{i_k}, \theta_{i_k}) - x_0\|_\infty \rightarrow \|x^* - x_0\|_\infty = r.$$

Since  $\hat{r}_n$  is the running maximum, monotone and bounded above by  $r$ , it converges almost surely to  $r$ .  $\square$

### Appendix A.6 Proof of Proposition 4.2 (Identification as Distance Minimization)

*Proof.* For singleton sets  $\{x\}$ , the Hausdorff distance reduces to:

$$d_H(\{x\}, \mathcal{M}) = \inf_{y \in \mathcal{M}} \|x - y\|_\infty.$$

Thus  $d_H(\{x\}, \mathcal{M}) < \varepsilon$  is equivalent to the existence of some  $y \in \mathcal{M}$  such that:

$$\|x - y\|_\infty < \varepsilon,$$

which is precisely the minimum-distance decision rule in supervised or unsupervised classification in Banach spaces.

Hence the perceptual decision reduces to verification of proximity to the compact perceptual manifold  $\mathcal{M}$ .  $\square$